Eur. Phys. J. D (2024) 78:85
https://doi.org/10.1140/epjd/s10053-024-00878-8

THE EUROPEAN PHYSICAL JOURNAL D

Regular Article - Atomic Physics

Zeeman spectroscopy of cadmium lines

S. Rathi[1], Ł. M. Sobolewski[2,a], L. Sharma[1], and J. Kwela[2]

[1] Indian Institute of Technology Roorkee, Roorkee, India
[2] Faculty of Mathematics, Physics and Informatics, Institute of Experimental Physics, University of Gdańsk, 80-308 Gdańsk, Poland

Received 23 April 2024 / Accepted 6 June 2024 / Published online 2 July 2024

Abstract. A Fabry–Perot interferometry was used to measure with a precision of about 10^{-4} the Landé factor values of the levels issued from the $5s5p$, $5s6d$, $5s6s$ and $5s7p$ configurations of cadmium. Fully relativistic MCDHF calculations taking into account Breit and QED effects were performed to interpret the results of the experiment performed on the cadmium isotope 114. In addition to the four experimental Landé g_J values, new theoretical results for 12 levels are reported for the first time.

1 Introduction

Cadmium is a soft silvery-white metal akin to zinc and mercury, the other stable metals within group 12. Being toxic in nature, cadmium has low exposure limits for humans. Cases of overexposure may occur even in environments where only minimal amounts of cadmium are present. This can explain the small number of experimental works on the structure of cadmium [1–10].

Cadmium and its counterparts in group 12 are often distinguished from transition metals due to the absence of partially filled d or f electron shells. With the atomic number (Z) of 48, naturally occurring cadmium comprises eight isotopes. Two of them are radioactive, and three are likely to decay, but this has not been measurably observed in laboratory conditions. The heavier isotopes decay mostly through beta emission. In the present work, we studied the pure isotope 114, the most abundant isotope. Spectral lines of this predominant isotope do not have hyperfine structure.

On another note, recently cadmium has emerged as a highly desirable candidate for optical lattice clocks [11–13] and also stands out as a key candidate for exploring new physics through King's plot nonlinearities [14]. The observation of these deviations may be a signature, for example, of a new boson mediating the interaction between electrons and neutrons.

First measurements of Landé g_J of $5s5p\ ^3P_1$ level of Cd I were carried out by Kohler and Thaddeus in 1964 [6]. Experimental and theoretical Landé g_J factor of the levels originating from $5s5p$ and $5s5d$ of Cd I are reported by Huet and Luc-Koenig [15]. Recently, theoretical multiconfiguration Dirac–Hatree–Fock (MCDHF) calculations on the Landé g_J factors of the $5s5p\ ^3P_{1,2}$ and $^1P_1$ states in Cd are taken into account as possible atomic clock states [16]. To our knowledge, no other major studies concerning the Landé g_J factors of Cd I are available in the literature.

In this work, we carried out the analysis of the Zeeman spectrum of Cd 114 by Fabry–Perot interferometry, which makes it possible to measure the Landé g_J factors of atomic levels with a precision of the order of 10^{-4}. The studies described below relate to the configuration levels $5s5p, 5s6d, 5s6s$ and $5s7p$ of cadmium. To support our experimental observations, we performed theoretical calculations of Landé g_J factor implementing the fully relativistic multiconfiguration Dirac–Hatree–Fock approach. The importance of including configuration mixing and relativistic effects to accurately define the wavefunction and subsequent calculations of the Landé g_J of the levels of Cd has been emphasized in the past [15,17]. Therefore, we constructed a detailed model by effectively considering electron correlations among the levels. We further incorporate the Breit and QED corrections, as these corrections become important for the accurate interpretation of measurements.

Overall, new experimental results of three levels are reported. Theoretical Landé g_J values for the 22 lowest states of Cd I have been computed. Among these, 12 values are entirely new, representing the first reported instances of their determination.

2 Experiment

Using Fabry–Perot interferometry, we examined the structure of five lines of cadmium in the range of 441.29–820.03 nm (see Table 1). The analysis of the spectra allowed the determination of Landé factor values of four levels, of which three are new.

[a] e-mail: lukasz.sobolewski@ug.edu.pl (corresponding author)

Table 1 Atomic lines of Cd I investigated in our study

Line (nm)	Upper level			Lower level		
	Energy (cm^{-1})	J	Parity	Energy (cm^{-1})	J	Parity
441.29894	53 310.101	0	e	30 656.087	1	e
466.2352	65 134.783	2	e	43 692.384	1	o
467.81493	51 483.980	1	e	30 113.990	0	o
734.56704	65 134.783	2	e	51 483.980	1	e
820.03089	65 501.412	1	o	53 310.101	0	e

e, even parity; o, odd parity

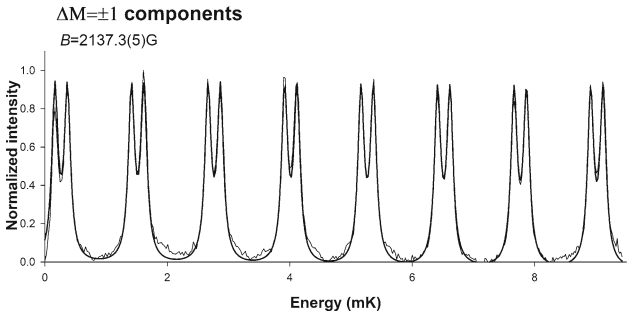

Fig. 1 Recorded interferogram (σ-view) of the 466.2352 nm line. The thick solid line represents the best computer-fitted line profile. The unit of energy is mK (milli-Kayser)

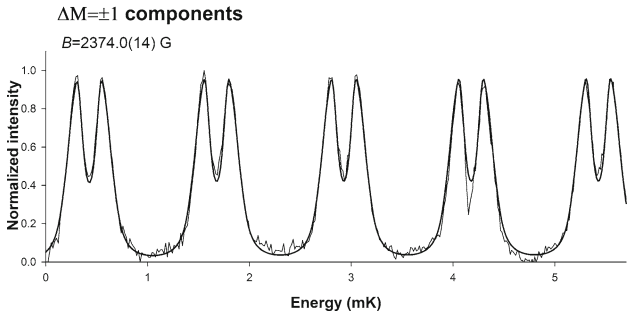

Fig. 2 Recorded interferogram (σ-view) of the 734.56704 nm line. The thick solid line represents the best computer-fitted line profile. The unit of energy is mK

A reliable fit of the Lande factor values for the π polarization spectra were impossible because the spectra consisted of only one broadened peak. We therefore abandoned the analysis of them. However, for the σ polarization, the spectra consisted of two well-separated peaks, the position of which was very sensitive to changes in the magnetic field value. We conducted observations for three different magnetic field values: 1964.0(23) G, 2137.3(5) G, and 2374.0(14) G. We determined the exact value of the magnetic field by observing the Zeeman splitting of the strongest 466.2352 nm line of cadmium in the tested range. For magnetic field calibration, we used g_J values from paper [15]. The measurements were repeated several (10–20) times in variable laboratory conditions. Examples of the spectra we recorded are shown in Figs. 1 and 2. The thin lines in the figures represent the experimental trace, while the thick solid lines represent the best computer fit. We used our own computer program described in detail in paper [18] for the fitting procedure, which had previously been tested on many observations of the Zeeman effect presented in a number of publications (see recent [19,20]).

3 Theoretical approach

We carried out a fully relativistic theoretical calculation of Landé g_J factor for Cd I pertaining to $5sns$, $5snp$, $5s5d$, $5s4f$ and $5s6d$ configurations with n ranging from 5 to 7. These configurations perfectly include the levels observed in the present experiment and the other necessary configurations needed to improve the accuracy of the results. Later in this study, we will refer to these states by multireference (MR) set.

For generating the atomic state wavefunction (ASF), the multiconfiguration Dirac–Hatree–Fock theory implemented in GRASP2018 [21] is applied. The theory of the MCDHF approach is described in Grant's book [22] and Jönsson et al. [23]. Briefly, in this approach, the ASFs (Ψ) for a given level of parity P and total quantum number J are given as linear combinations of configuration state functions (CSFs) that are formed through symmetry-adapted linear combinations of Slater determinants of one-electron Dirac orbitals.

For our study, we represent the effective Hamiltonian for an N electron system as,

$$H_{\text{eff}} = \sum_{i=1}^{N} h^D(i) + \sum_{j>i=1}^{N} V_{ij}, \tag{1}$$

where h^D is the one-electron Dirac operator. The interaction between the atomic electrons caused by the Breit VB (magnetic and retardation effects) and the Coulomb VC interactions are represented by the term V_{ij}, which can be stated as [23],

$$V_{ij} = VC_{ij} + VB_{ij}, \tag{2}$$

The MR set is optimized using the relativistic self-consistent field (RSCF) approach for the Hamiltonian defined in Eq. 1. During this optimization, only the

Table 2 Present MCDHF energies and their comparison with the corresponding NIST values for Cd I along with the *LS* composition of each level

Configuration	Term	J	NIST (cm^{-1})	MCDHF^{tw} (cm^{-1})	*LS* composition*
$5s^2$	^1S	0	0	0	0.93
$5s5p$	^3P	0	30113.990	30177	0.96
$5s5p$	^3P	1	30656.087	30659	0.93
$5s5p$	^3P	2	31826.952	31675	0.88 + 0.08 $5s6p\ ^3P$
$5s5p$	^1P	1	43692.384	44100	0.92
$5s6s$	^3S	1	51483.980	51978	0.74 + 0.23 $5s7s\ ^3S$
$5s6s$	^1S	0	53310.101	52702	0.79 + 0.18 $5s7s\ ^1S$
$5s6p$	^3P	0	58390.9	58463	0.90 + 0.07 $5s7p\ ^3P$
$5s6p$	^3P	1	58461.6	58531	0.64 + 0.23 $5s7p\ ^1P$ + 0.08 $5s6p\ ^1P$
$5s6p$	^3P	2	58635.7	58689	0.68 + 0.21 $5s7p\ ^3P$
$5s5d$	^1D	2	59219.734	59207	0.51 + 0.32 $5s5d\ ^3D$ + 0.06 $4d^{10}5p^2\ ^1D$
$5s5d$	^3D	1	59485.768	59358	0.53 + 0.45 $5s6d\ ^3D$
$5s5d$	^3D	2	59497.868	59369	0.31 + 0.27 $5s6d\ ^3D$ + 0.21 $5s5d\ ^1D$
$5s5d$	^3D	3	59515.990	59376	0.79 + 0.19 $5s6d\ ^3D$
$5s6p$	^1P	1	59907.28	59513	0.43 + 0.31 $5s7p\ ^3P$ + 0.20 $5s7p\ ^1P$
$5s7s$	^3S	1	62563.435	62067	0.73 + 0.25 $5s6s\ ^3S$
$5s7s$	^1S	0	63086.896	62371	0.63 + 0.33 $5s6s\ ^1S$
$5s7p$	^3P	0	64995.9	64600	0.90 + 0.07 $5s6p\ ^3P$
$5s7p$	^3P	1	65025.5	64626	0.63 + 0.24 $5s6p\ ^1P$ + 0.09 $5s7p\ ^1P$
$5s7p$	^3P	2	65093.702	64685	0.76 + 0.21 $5s6p\ ^3P$
$5s6d$	^1D	2	65134.783	65274	0.52 + 0.38 $5s6d\ ^3D$ + 0.05 $5s5d\ ^1D$
$5s6d$	^3D	1	65353.372	65475	0.56 + 0.42 $5s5d\ ^3D$
$5s6d$	^3D	2	65358.881	65475	0.31 + 0.28 $5s5d\ ^3D$ + 0.21 $5s6d\ ^1D$
$5s6d$	^3D	3	65367.227	65486	0.74 + 0.21 $5s5d\ ^3D$
$5s7p$	^1P	1	65501.412	65625	0.44 + 0.31 $5s6p\ ^3P$ + 0.21 $5s6p\ ^1P$
$5s4f$	^3F	2	65586.0	65984	0.98
$5s4f$	^3F	3	65586.0	65986	0.56 + 0.43 $5s4f\ ^1F$
$5s4f$	^1F	3		65994	0.57 + 0.42 $5s4f\ ^3F$

*The leading term in the *LS* composition represents the contribution of the ASF itself
^{tw}This work

Coulomb potential is taken into account, while the Breit interaction is included later as a perturbative correction. In the RSCF step, the radial Dirac orbitals and the mixing coefficients are optimized to self-consistency.

Further, for an accurate theoretical description of the Landé g_J factor, it is important to take into account the correction arising from the radiative QED effects, viz. vacuum polarization (VP) and self-energy (SE) corrections. In the present study, these corrections are included perturbatively in the relativistic configuration interaction (RCI) approach and are not included in the RSCF procedure. The vacuum polarization effects are considered by including the Uehling potential. For the self-energy (one-loop) correction term, we used the screened-hydrogenic approximation. The screening coefficient is estimated in this approach by comparing the analogous density of a hydrogenic orbital with the Dirac–Fock wavefunction density near the nucleus ($r \leq 0.0219 \cdot a_0$, where a_0 is the Bohr's radius). Additional details on SE and how it is incorporated in GRASP2018 are available in [23,24].

To account for the electron correlation effects, single–double–triple excitations of electrons from the MR subshells to higher virtual orbitals are considered. We included virtual orbitals up to $n = 11$ with our active layers defined as $A_1 = \{8s,\ 8p,\ 7d,\ 5f\}$, $A_2 = \{9s,\ 9p,\ 8d,\ 6f\}$, $A_3 = \{10s,\ 10p,\ 9d,\ 7f\}$, $A_4 = \{11s,\ 11p,\ 10d,\ 8f\}$ and $A_5 = \{11s,\ 11p,\ 11d,\ 9f\}$.

Valence–valence correlations are included by allowing all possible excitation from the valence orbitals $5s\{nl, 5d, 6d, 5f\}$ with $n = 5-7$ and $l = s, p$. To include the effect of core orbitals, we allowed only a single excitation from the core orbitals, $4s, 4p, 4d$. We limited the core excitations by allowing at most one excitation at a time from a core orbital in order to maintain control over the significant expansion of the CSFs. A further constraint is imposed on the $2J$ value, which has a maximum value of 6 in the present calculations.

This results in the creation of 19,22,815 CSFs in total. This procedure successfully integrates correlations from the valence and core orbitals in our calculations [25]. Furthermore, this process is quite rigorous and capable of effectively capturing the inter-configuration interactions. In addition, to mitigate computational strain and monitor convergence, the calculations are done in a layer-by-layer fashion, optimizing the newly added

Table 3 Determined experimental and theoretical values of Landé g_J - factors of the investigated levels of Cd I

					Experimental		Theoretical	
Energy (cm^{-1})	Designation	J	Line	g_J^{LS}	g_J^{tw}	g_J^{others}	g_J^{tw}	g_J^{others}
43 692.374	$5s5p\ ^1P$	1	430.66718	1.0		1.0013(2) [15]	**1.00030**	1.001004 [16]
								1.00134 [15]
30 656.087	$5s5p\ ^3P$	1	441.29894	1.5	**1.5027(21)**	1.499846(10) [6]	**1.50068**	1.499006 [16]
						1.4997(3) [15]		1.49976 [15]
31 826.952	$5s5p\ ^3P$	2	–	1.5		1.5007(3) [15]	**1.50010**	1.499968[16]
								1.50112 [15]
65 134.783	$5s6d\ ^1D$	2	466.234	1.0	**0.9953(13)**		**1.00004**	
51 483.980	$5s6s\ ^3S$	1	467.81493	2.0	2.0294(67)			
			734.56704		1.982(12)			
					2.018(15)*		**2.00224**	
65 501.412	$5s7p\ ^1P$	1	820.03089	1.0	**0.9929(32)**		**1.00082**	
59 219.734	$5s5d\ ^1D$	2		1.0		0.9998(1) [15]	**1.00003**	1.00000 [15]
59 485.768	$5s5d\ ^3D$	1		0.5		0.4987(3) [15]	**0.49878**	0.49882 [15]
59 497.868	$5s5d\ ^3D$	2		1.167		1.1669(2) [15]	**1.16700**	1.16702 [15]
59 515.990	$5s5d\ ^3D$	3		1.34		1.3335(3) [15]	**1.33408**	1.33411 [15]
58 461.6	$5s6p\ ^3P$	1		1.5			**1.49592**	
58 635.7	$5s6p\ ^3P$	2		1.5			**1.50112**	
59 907.28	$5s6p\ ^1P$	1		1.0			**1.00067**	
62 563.435	$5s7s\ ^3S$	1		2.0			**2.00225**	
65 025.5	$5s7p\ ^3P$	1		1.5			**1.50085**	
65 093.702	$5s7p\ ^3P$	2		1.5			**1.50112**	
65 353.372	$5s6d\ ^3D$	1		0.5			**0.49887**	
65 358.881	$5s6d\ ^3D$	2		1.167			**1.16699**	
65 367.227	$5s6d\ ^3D$	3		1.34			**1.33408**	
65 586.0	$5s4f\ ^3F$	2		0.67			**0.66591**	
65 586.0	$5s4f\ ^3F$	3		1.0834			**1.08351**	
	$5s4f\ ^1F$	3		1.0			**0.99999**	

*Weighted mean value

orbitals and keeping the others fixed. A similar procedure has been used in our previous works [20,26].

Finally, after obtaining optimized wavefunctions for the configurations in our MR set, we computed the Landé g_J factors expressed as [27,28],

$$g_J = \frac{2}{\sqrt{J(J+1)}}\langle\Psi\|\sum_{j=1}^{N}\left[\sqrt{-1}\frac{\sqrt{2}}{2\alpha^2}r_j(\boldsymbol{\alpha}_j\mathbf{Y}_j^{(1)})^{(1)} + \frac{g_s-2}{2}\beta_j\chi_j\right]\|\Psi\rangle. \quad (3)$$

Here α, χ and $\mathrm{Y}^{(1)}$ are the fine structure constant, relativistic spin matrix and vector spherical harmonics, respectively. α_j and β_j correspond to the Dirac matrices defined as,

$$\alpha_j = \begin{pmatrix} 0 & \sigma_j \\ \sigma_j & 0 \end{pmatrix},\ \beta = \begin{pmatrix} I & 0 \\ 0 & -I \end{pmatrix}. \quad (4)$$

here σ_j and I represent the Pauli matrices and identity matrix, respectively. The second term in Eq. 3 is the Schwinger QED corrections to the operator defined in the first term accounting for the QED effects in the electron's gyromagnetic factor. The value of g_s in this case is 2.00232.

4 Results and discussion

Theoretical energies calculated in the current study are given in Table 2 and compared with the available results at the National Institute of Standards and Technology Atomic Spectra Database (NIST ASD), USA [29]. A good agreement between the two sets of energies is evident, characterized by a root mean square deviation of 314 cm^{-1}. This alignment supports the fact that the bound state wavefunctions of the concerned levels are generated accurately, incorporating the major relativistic effects. Further, to show the level mixing between different levels, in Table 2, we also present the LS composition of all the concerned levels. Only the CSFs with the most significant contributions are included, with a limit of up to a maximum of three CSFs.

In Table 3, the Landé g_J values from our current theoretical calculations for A_5 are listed in column eight. To demonstrate the convergence of our calculated Landé g_J values, we present the mean and standard deviation (StD) of the absolute differences between the

Table 4 The mean and standard deviation of the absolute difference of Landé g_J factors calculated from two consecutive active layers

	$\lvert A_2 - A_1\rvert$	$\lvert A_3 - A_2\rvert$	$\lvert A_4 - A_3\rvert$	$\lvert A_5 - A_4\rvert$
Mean	1.228E−02	2.635E−03	2.977E−04	7.849E−06
StD	2.175E−02	4.062E−03	5.554E−04	1.599E−05

values from two consecutive layers in Table 4. The systematic decrease in the mean values indicates convergence, with each layer showing progressively smaller differences from the previous one. Similarly, the StD values also exhibit a decreasing trend, suggesting reduced variability in the differences, thereby supporting the observed convergence. The difference between the last two layers ($|A_5 - A_4|$) decreases to the order of 10^{-6}, explaining the accuracy of our theoretical values to the fifth decimal place.

The experimental results, along with their measurement uncertainties of our experimental studies, are presented in the fifth column of Table 3. Numbers in brackets indicate statistical errors corrected by the Student's t-distribution coefficients [30]. Statistical errors come from the analysis of approximately 20 interferograms obtained for each of the tested lines under variable laboratory conditions. In the case of level $5s6s\ ^3S_1$, the Landé g_J value was obtained with higher reliability as a weighted mean from the observation of two lines. As it can be seen from Table 3, the results of our measurements are consistent with previous experimental data. Further, our experimental and theoretical outcomes from this investigation exhibit notable agreement.

Examining Table 3, we can also say that the present theoretical results are able to effectively interpret the experimental results from this as well as previous experimental studies of [15]. This also implies that the relativistic effects and configuration mixing are incorporated efficiently. Furthermore, Table 3 presents a comparative analysis between our current theoretical results and previously reported theoretical values of [15], as well as recent theoretical findings in [16]. Overall, the three studies show satisfactory agreement. Moreover, new theoretical Landé g_J values have been computed for selected levels of $5s6p$, $5s7s$, $5s7p$, $5s6d$, and $5s4f$ configurations, as detailed in Table 3.

Additionally, we have included the pure LS Landé g_J-factor in Table 3. The deviation between the relativistic and pure LS Landé g_J values can serve as an indicator of level mixing and influence of relativistic effects.

5 Conclusion

In this work, we present the results of Fabry–Perot interferometry measurements of the Landé factor for four levels of the cadmium atom.

To interpret the present experimental observations, theoretical calculations were performed. MCDHF theory, with careful consideration of Breit and QED effects, was used to calculate the Landé g_J factors for 22 levels of Cd I. The present theoretical results are in good agreement with the experimental observations. Within this study, we present new experimental Landé g_J values for three levels. Additionally, we introduce 12 new derived theoretical values, filling a gap where no previous experimental or theoretical data existed.

Acknowledgements S.R. and L.S. would like to thank the National Supercomputing Mission (NSM) for providing computing resources of "PARAM Ganga" at the Indian Institute of Technology Roorkee, implemented by C-DAC and supported by MeitY and DST, Government of India.

Author contributions

Authors S. Rathi and L. Sharma have contributed to the theoretical part of this paper. Ł. Sobolewski and J. Kwela have contributed to the experimental part of this paper. Paper editing was done jointly by all authors.

Data availability statement This manuscript has no associated data or the data will not be deposited. [Authors' comment: All the data associated with this work is provided in the manuscript.]

References

1. L.E. Kinsler, W.V. Houston, The value of e/m from the Zeeman effect. Phys. Rev. **45**, 104 (1934)
2. J.B. Green, D.E. Gray, The Paschen-Back Effect. I. L-S Coupling; the ^3P ^3D Multiplets of Zn and Cd. Phys. Rev. **45**, 273 (1934)
3. A.G. Shenstone, J.T. Pittenger, Cadmium spectra. J. Opt. Soc. Am. **39**(3), 219–225 (1949)
4. K. Burns, K.B. Adams, Energy levels and wavelengths of natural cadmium and of cadmium-114. J. Opt. Soc. Am. **46**, 94–99 (1956)

5. W. Faust, M. McDermott, W. Lichten, Hyperfine structure of the metastable $^3P_2$ State of Cd^{111} and Cd^{113}. Phys. Rev. **120**, 469 (1960)
6. R. Kohler, P. Thaddeus, g_J of the $(5s5p)$ $^3P_1$ level of Cd and the $(6s6p)$ $^3P_1$ level of hg by high-field double resonance. Phys. Rev **134**, 5A (1964)
7. W.R.S. Garton, J.P. Connerade, Absorption spectra of Zn I, Cd I, and Hg I in the vacuum ultraviolet. Astrophys. J. **155**, 667–675 (1969)
8. A. Nadeem, M. Nawaz, S. Hussain, S.A. Bhatti, M.A. Baig, Two-step laser spectroscopy of the highly excited even-parity levels of cadmium. J. Phys. B **38**, 867–875 (2005)
9. P. Maslowski et al., The hyperfine and isotope structure of the Cd intercombination line—revisited. Eur. Phys. J. D **51**, 295–302 (2009)
10. N. Frömmgen et al., Collinear laser spectroscopy of atomic cadmium. Eur. Phys. J. D **69**, 164 (2015)
11. A. Yamaguchi, M.S. Safronova, K. Gibble, H. Katori, Narrow-line cooling and determination of the magic wavelength of Cd. Phys. Rev. Lett. **123**(11), 113201 (2019)
12. Y. Kaneda, J.M. Yarborough, Y. Merzlyak, A. Yamaguchi, K. Hayashida, N. Ohmae, H. Katori, Continuous-wave, single-frequency 229 nm laser source for laser cooling of cadmium atoms. Opt. Lett. **41**(4), 705–708 (2016)
13. J.S. Schelfhout, J.J. McFerran, Multiconfiguration Dirac–Hartree–Fock calculations for Hg and Cd with estimates for unknown clock-transition frequencies. Phys. Rev. A **105**(2), 022805 (2022)
14. B. Ohayon, S. Hofsäss, J.E. Padilla-Castillo, S.C. Wright, G. Meijer, S. Truppe, K. Gibble, B.K. Sahoo, Isotope shifts in cadmium as a sensitive probe for physics beyond the standard model. New J. Phys. **24**(12), 123040 (2022)
15. M. Huet, E. Luc-Koenig, Facterurs de Landé des niveaux des configurations 5s5p et 5s5d de Cd I. Opt. Commun. **40**, 5 (1982)
16. B. Lu, H. Chang, Theoretical calculations on Landé g-factors and quadratic Zeeman shift coefficients of $nsnp$ $^3P_0$ clock states in Mg and Cd optical lattice clocks. Chin. Phys. B **23**, 013101 (2023)
17. M. Chantepie, J.L. Cojan, J. Landais, B. Laniepce, Lifetimes of the $n\,^1S_0$ and $n\,^1D_2$ states of cadmium. J. Phys. **41**, L433 (1980)
18. D. Grabowski, R. Drozdowski, J. Kwela, J. Heldt, Hyperfine structure and Zeeman effect studies in the $6p7p - 6p7s$ transitions in Bi II. Z. Phys. D **38**, 289–293 (1996)
19. Ł.M. Sobolewski, L. Windholz, J. Kwela, Landé g_J -factors of Nb I levels determined by laser spectroscopy. J. Quant. Spect. Rad. Transf. **249**, 107015 (2020)
20. Ł.M. Sobolewski, S. Rathi, L. Sharma, L. Windholz, J. Kwela, Laser optogalvanic spectroscopy of lead lines-Isotope shifts and hyperfine structure studies. J. Quant. Spectrosc. Radiat. Transf. **316**, 108901 (2024)
21. C.F. Fischer, G. Gaigalas, P. Jönsson, J. Bieroń, GRASP2018-A Fortran 95 version of the general relativistic atomic structure package. Comput. Phys. Commun. **237**, 184–187 (2019)
22. I.P. Grant, *Relativistic Quantum Theory of Atoms and Molecules: Theory and Computation* (Springer, New York, 2007)
23. P. Jönsson, M. Godefroid, G. Gaigalas, J. Ekman, J. Grumer, W. Li, J. Li, T. Brage, I.P. Grant, J. Bieroń, C.F. Fischer, An introduction to relativistic theory as implemented in GRASP. Atoms **11**(1), 7 (2022)
24. J.A. Lowe, C.T. Chantler, I.P. Grant, Self-energy screening approximations in multi-electron atoms. Radiat. Phys. Chem. **85**, 118–123 (2013)
25. P. Jönsson, G. Gaigalas, C.F. Fischer, J. Bieroń, I.P. Grant, T. Brage, J. Ekman, M. Godefroid, J. Grumer, J. Li, W. Li, GRASP manual for users. Atoms **11**(4), 68 (2023)
26. S. Rathi, Ł.M. Sobolewski, L. Sharma, J. Kwela, Zeeman spectroscopy of tellurium. J. Quant. Spectrosc. Radiat. Transf. **309**, 108704 (2023)
27. S. Verdebout, C. Naze, P. Jönsson, P. Rynkun, M. Godefroid, G. Gaigalas, Hyperfine structures and Landé g_J-factors for $n = 2$ states in beryllium-, boron-, carbon-, and nitrogen-like ions from relativistic configuration interaction calculations. At. Data Nucl. Data Tables **100**(5), 1111–1155 (2014)
28. M. Andersson, P. Jönsson, HFSZEEMAN—a program for computing weak and intermediate field fine and hyperfine structure Zeeman splittings from MCDHF wave functions. Comput. Phys. Commun. **178**(2), 156–170 (2008)
29. A. Kramida, Y. Ralchenko, J. Reader, and NIST ASD Team, NIST Atomic Spectra Database (ver. 5.11). National Institute of Standards and Technology, Gaithersburg. https://physics.nist.gov/asd [2024, April 17]. https://doi.org/10.18434/T4W30F
30. NIST/SEMATECH e-Handbook of Statistical Methods. http://www.itl.nist.gov/div898/handbook (2024)